Theoretical Prediction and Experimental Measurement of Isothermal Extrudate Swell of Monodisperse and Bidisperse Polystyrenes

Ben Robertson [a], Richard L. Thompson

Department of Chemistry, Durham University, Durham, DH1 3LE, United Kingdom

Tom C. B. McLeish

Department of Physics, Durham University, Durham, DH1 3LE, United Kingdom

Ian Robinson

Lucite International, Wilton, Redcar, TS10 4RF United Kingdom

Abstract

This paper describes the theoretical prediction, finite element simulation and experimental studies of extrudate swell in monodisperse and bidisperse polystyrenes. We present a molecular approach to understanding extrudate swell using the tube-model-based Rolie-Poly constitutive equation within a Lagrangian finite element solver. This yields theoretical predictions of swelling which show a close universality: the molecular weight dependence of the swelling can be removed when the flow speed is scaled by the Rouse Weissenberg number. The roles that both chain orientation and stretch play in determining extrudate swell are clearly identifiable from plots of swelling ratio against each Weissenberg number. We also present isothermal extrusion experiments on the same polymers and can obtain good predictions well into the strong chain stretching regime. The predictions for swelling ratios match those from experiments up to Rouse Weissenberg numbers of ~7, above which swelling is over-predicted by the Rolie-Poly equation.

I. INTRODUCTION

Predictions of extrudate swell have been sought for many years, frequently with the intent to relate its magnitude to measurable rheometrical quantities. For example, Tanner (1970) [1] related swelling out of a long capillary to measurement of first normal stress difference and shear stress:

[a] Email: Benjamin.robertson@durham.ac.uk

$$\frac{D_e}{d} = [1 + \frac{1}{2}(\frac{N_1}{2\tau_w})^2]^{\frac{1}{6}} + 0.1 \quad (1)$$

Here τ_w is the shear stress at the capillary wall and N_1 is the first normal stress difference across the capillary. D_e is the maximum diameter of the extrudate at steady state flow and d is the diameter of the capillary used for extrusion. This equation has proven useful in roughly predicting extrudate swell although it neglects several factors which are present in practical extrusion experiments:

i. Die entry and exit effects are ignored (as the die is assumed to be infinitely long).
ii. The influences of gravity and surface tension are not included.
iii. The swelling profile cannot be predicted, only the maximum swelling ratio.

The constant 0.1 is added empirically to improve fit to experimental data. This is required because the elastic recovery arguments used in the rest of the equation fail to predict the Newtonian swelling ratio of 1.1. The factor was changed to 0.13 in later papers.[2] The fraction D_e/d is referred to as the B value.

Other theories have used similar approaches with varying advantages and disadvantages, for example using entry/exit pressure drops and values for the wall shear stress. Liang *et al* [3] stated that B was a linear function of wall shear stress:

$$B = f_1 + f_2\tau_w \quad (2)$$

The constants f_1 and f_2 are material specific constants related to the elasticity of the polymer and τ_w is the wall shear stress. This equation fits experimental data well for filled rubber compounds although not for very high shear rates.

The die exit pressure drop was predicted by Liang [4] to affect extrudate swell.

$$B = [1 + \frac{3\Delta P_{exit}}{\tau_w}]^{1/4} \quad (3)$$

where ΔP_{exit} is the pressure drop across the die exit. This equation fits experimental data for high density polyethylene (HDPE) melts best at high shear rates with significant deviations at lower shear.

Seriai et al [5] removed the long die condition by experimentally investigating the *l:d* ratio (the ratio of the capillary length *l* to its diameter *d*) of the capillary and the capillary residence time. For longer dies the extrudate swell was found to drop off, becoming a function of the capillary wall shear rate. This is due to stress relaxation along the extruder length becoming more effective as *l:d* increases.

The conditions into which the extrusion occurs are also important. If the surrounding temperature is lower than the extrudate then cooling will result in lower extrudate swell. When the extrudate exits the heated die into the 'cold' medium it will contract thermally, causing shrinkage. The flow properties of the polymer will also change. The inner portion of the extrudate will have a lower viscosity than the cooler, outer portion which may cause swelling .[6] On the other hand, swelling will be arrested if the polymer is cooled through its glass transition (or crystallised in the case of semicrystalline polymers, such as HDPE), potentially trapping stresses within the extrudate. This effect has historically been corrected for by annealing the extrudate. The disadvantage of this method is that it is difficult to measure change in extrudate swell over time and that measured diameters must be corrected for thermal expansion/cooling. Extrusion into a heated oil bath [7] solves the heating/cooling problem but raises problems involving penetration of the oil into the extrudate and surface tension effects. An optimal way to avoid all these problems is to perform the whole extrusion isothermally, as is done in this work.

Yang et al [8] used a capillary rheometer to study the molecular weight dependence of the extrudate swell. In these experiments the extrudate was cooled immediately on extrusion, then annealed in a heated oil bath for a fixed period of time to measure the stress relaxation within the extrudate as a function of annealing time. They found that the swelling ratio at a specific annealing time and shear rate decreases with increasing molecular weight of the polymer. However, when the time was scaled by the polymer relaxation time the data reduced to a single curve, meaning extrudate swell was independent of molecular weight. This relaxation time was calculated from the polymer melt viscosity rather than using polymer relaxation times taken from molecular theory. They also found that extrudate swell decreases with increasing die length but additionally decreases with the addition of slip at the die exit.

It is therefore important to understand extrudate swell on a deeper level than simple theories based on normal stresses or pressure drops as any change in the amount of unrelaxed stress at the die exit can have significant effects on the swell behaviour. Both industrial application

and an understanding of polymer process science seek a way of predicting extrudate swell at a wide range of shear rates using molecular characteristics of the polymer known from its synthesis.

Such an approach requires two major steps: First, a constitutive model for the material must be employed, consistent with the molecular physics and chemical structure of entangled melts. Second, this formulation should be solved for the specific complex flow-fields encountered in extrusion. It is therefore necessary to use a fluid dynamics package capable of computing viscoelastic flows. This has been attempted in the context of extrudate swell using the K-BKZ [9], Phan-Thien Tanner (PTT) [10], Oldroyd-B [11] and the Pom-Pom [12] models amongst others. In 2011 Ganvir *et al* [12] used a Lagrangrian-Eulerian method and the XPP (eXtended Pom-Pom)[13] model. They reported reasonable agreement with experiment for commercial grade polydisperse polyethylenes although the simulations consistently over-predicted swelling due to non-isothermal effects

Most of the experiments performed thus far have included a complicating factor making accurate prediction of extrudate swell difficult. Polydispersity and branched architectures tend to smooth out rheological features such as signatures of chain reptation and chain stretch, making the underlying cause of the observed phenomena harder to see. To develop an understanding of the underlying causes of extrudate swell therefore it is preferable to test any model using well characterised, monodisperse, linear melts. However, given the difficulty in synthesising large volumes of these materials it is necessary to perform small (gram) scale experiments rather than the kilogram scales that are required for industrial extruders. The tube theory of entangled polymer melts was itself developed through rheometry on small samples of monodisperse linear, star, comb and other controlled architecture polymers. [14] The same methodology has recently been successfully extended to complex flows. For example, Graham et al [15] and Bent et al [16] performed recirculating flow cell experiments on ~200 g scales to compare the predictions of the Rolie-Poly equation to neutron scattering and birefringence experiments of monodisperse polystyrenes.

The ability to perform rheometrical measurements under processing conditions on smaller scale than the recirculating flow cell or a conventional capillary rheometer is beneficial in such circumstances, where it is difficult to manufacture larger quantities of a polymer. To this end the Multi-Pass Rheometer (MPR) was developed in Cambridge.[17] The MPR consists of two hydraulically driven pistons, each inserted into a barrel filled with polymer. In-

between the upper and lower barrels is placed a specially designed test section into which a variety of test pieces can be inserted. Quartz viewing windows are also inserted into the test section to allow visualisation of the flow during the test. The MPR can perform experiments using as little as 10 g of polymer and has been adapted for contraction-expansion, extrusion, capillary and cross slot flows. In the work reported here, the MPR is used in a novel mode in which the lower chamber is originally nitrogen filled, enabling controlled visualisation of isothermal extrusion.

Accurate simulation of these different flows requires modelling of both linear and non-linear rheology. The basic component of rheological linear response is the Maxwell model, which fits the linear rheological data to a series of single exponential relaxation processes:

$$\sigma(t) = \sigma_0 e^{-t/\tau} \tag{4}$$

where $\sigma(t)$ is the stress at time t, $\sigma(0)$ is the starting stress and τ is the relaxation time of the mode. It is possible to sum up a series of these 'modes' to model a series of relaxation times. These Maxwell modes can be summed together to give a full linear viscoelastic spectrum. So, over i modes:

$$G_i^{'}(\omega) = G_i\left(\frac{(\omega\tau_i)^2}{1+(\omega\tau_i)^2}\right)$$

and (5)

$$G_i^{''}(\omega) = G_i\left(\frac{\omega\tau_i}{1+(\omega\tau_i)^2}\right)$$

where G' and G'' are the storage and loss moduli of the polymer, ω is the measurement frequency G_i is the modulus of the Maxwell mode and τ_i is the relaxation time of the mode.[18]

The theory of Likhtman-McLeish specifies a particular example of the general Maxwell model in the case of monodisperse, linear, entangled polymer melts, using molecular tube theory to predict linear rheology and extract relaxation timescales for the polymer melt. In particular it describes how to obtain the terminal reptation time, τ_d and the Rouse relaxation time, τ_R [19] from the entanglement time, τ_e and the number of entanglements per molecule, Z.

$$\tau_d = 3\tau_e Z^3\left(1-\frac{3.38}{\sqrt{Z}}+\frac{4.17}{Z}-\frac{1.55}{Z^{3/2}}\right)$$
$$\tau_R = \tau_e Z^2 \tag{6}$$

The Rolie-Poly ('Rouse Linear Entangled Polymer') constitutive equation, used to model non-linear rheology, was derived by Likhtman and Graham in 2003 [20]. It is a simplification of the 'GLAMM' theory by Graham *et al*. in the form of a differential rheological constitutive equation, which embodies entanglement tube theory into a fully non-linear constitutive equation valid from slow flow into the strongly chain-stretching regime. [21] The full theory includes terms for chain orientation; chain stretch and convective constraint release (CCR) as well as terms for coupling between these.[14] This is transformed into a much simpler equation applicable as it stands to a monodisperse melt, or to each fraction in a polydisperse melt, where the Rolie-Poly differential model becomes a non-linear extension of each of the linear relaxation modes of the material.

For a monodisperse melt, or for each fraction that undergoes chain-stretch, the stress is calculated using the Rolie-Poly equation;

$$\frac{d\boldsymbol{\sigma}}{dt} = \boldsymbol{\kappa}\cdot\boldsymbol{\sigma} + \boldsymbol{\sigma}\cdot\boldsymbol{\kappa}^T - \frac{1}{\tau_d}(\boldsymbol{\sigma}-\mathbf{I}) - \frac{2}{\tau_R}\left(\frac{\lambda-1}{\lambda}\right)\boldsymbol{\sigma} - \frac{2\beta}{\lambda\tau_R}\left(\frac{\lambda-1}{\lambda}\right)(\boldsymbol{\sigma}-\mathbf{I})) \tag{7}$$

where $\boldsymbol{I}$ is the identity matrix, $\boldsymbol{\kappa}$ is the velocity gradient tensor, $\boldsymbol{\sigma}$ is the local stress tensor, λ is the chain stretch; calculated from the scalar trace of the local stress tensor $\lambda = \sqrt{tr(\boldsymbol{\sigma})/3}$ and β is a parameter determining the strength of constraint release. This is kept constant at β=0.5 as recommended in earlier papers on CCR[22] and is in line with previous uses of the Rolie-Poly model with linear polymers. [21] τ_d is the reptation time of the mode and τ_R is its Rouse relaxation time. The key feature of the Rolie-Poly model encompassing chain-stretch is that the constitutive representation of even a single monodisperse fraction carries two relaxation times, a longer one (reptation) controlling the orientation of chain segments, and a faster one (Rouse) relaxing the chain stretch (mathematically appearing as a function of the trace of the stress tensor). In purely linear response, only the relaxation characterised by τ_d appears (which allows a non-linear theory to be 'generated' by a set of linear relaxation modes by extending each one with a Rolie-Poly structure). A simpler alternative form of the model that removes the nonlinearity due to chain stretch is used as non-linear extensions of the high-frequency modes, since these arise

predominantly from sub-chain structures that do not stretch in the flow rates of our experiments:

$$\frac{d\boldsymbol{\sigma}}{dt} = \boldsymbol{\kappa}\cdot\boldsymbol{\sigma} + \boldsymbol{\sigma}\cdot\boldsymbol{\kappa}^{T} - \frac{1}{\tau_d}(\boldsymbol{\sigma} - \mathbf{I}) - \frac{2}{3}tr(\boldsymbol{\kappa}\cdot\boldsymbol{\sigma})(\boldsymbol{\sigma} + \beta(\boldsymbol{\sigma} - \mathbf{I})) \tag{8}$$

The resulting model using multiple stretching and non-stretching Rolie-Poly elements can be used to calculate the stress deformation and chain stretch at any point in a flow simulation by calculating the change in stress across each simulation time step.

The Rolie-Poly equation has provided accurate flow predictions of monodisperse entangled linear polymer melts especially for MPR flow studies performed as part of the Microscale Polymer Processing (μPP) projects.[23-25] The μPP projects produced several tools based on these theories to aid analysis and use of rheometrical data, which we employ in this work. Firstly, the analysis toolkit *RepTate* [26] allows time-temperature superposition of linear and non-linear rheometrical data and fitting to these data using, amongst others, the linear and non-linear theories introduced above.

Secondly, the Lagrangian finite element solver *flowSolve* allows the parameters generated by *RepTate* to be used for flow modelling and computation. [27] *The flowSolve* program uses a starting mesh of triangles to simulate the polymer flow. At each step in the simulation the velocity of each grid point is calculated. The velocity gradient is assumed to be constant between each pair of connected grid points. The stress is then calculated for each triangle using these velocity gradients and a constitutive equation such as the Rolie-Poly or Pom-Pom equations. The Rolie-Poly equation is used for linear polymers whereas the Pom-Pom equation is used mainly for branched polymers.[20, 28] The mesh points are then moved according to their velocities. This will result in a deformation of the triangular mesh throughout the simulation. As with any Lagrangian solver, regular remeshing is required to maintain a regularly shaped triangular mesh which accurately portrays the fluid flow and accurately captures the stress history throughout the simulation. The velocities and velocity gradient tensors are calculated using standard equations for mass and momentum conservation in the non-inertial limit:

$$\begin{aligned} \nabla_i v_i &= 0 \\ \nabla_j \sigma_{ij} &= \nabla_i p - \mu \nabla^2 v_i \end{aligned} \tag{9}$$

where μ is a Newtonian viscosity term formed from the fast 'solvent' modes of the simulation (in a melt these may arise from viscoelastic material but possessing relaxation times much faster than any of the deformation rates in the flow) and *v* is the velocity of the point at a particular time step.

The *flowSolve* program allows simulation of a variety of different flow geometries via incorporation of both fixed and moving boundary walls with slip or no-slip boundary conditions. In the case of free surface flows the polymer parameters can be altered to include gravity and surface tension.

flowSolve has been used in an earlier form to predict flow of polyethylenes through a slit. [29] It could predict the stress birefringence at the flow inlet and outlet and has also been used to predict stress birefringence in cross slot flow. [30] The predictions of the Pom-Pom model break down at high shear rates due to flow asymmetry and flow memory effects. The μPP project used *flowSolve* to predict flow properties at specific points of interest in the flow, for example comparison to neutron scattering data for flow past re-entrant corners. [31] Work on constriction flows in the MPR is relevant here, describing how the entry and exit flows of polystyrene through a slit vary as a function of Weissenberg number (the deformation rate made dimensionless with respect to the dominant relaxation time of the material).[27] These studies describe the three regimes that emerge from the two relaxation times of Rouse and reptation processes. We will therefore find it useful to define two Weissenberg numbers, one with respect to the reptation time of a linear entangled chain ($W_d = \tau_d \times \dot{\gamma}$), and one with respect to its Rouse (stretching) time ($W_R = \tau_R \times \dot{\gamma}$):

$$\begin{array}{cc} W_d < 1 & \text{Linear response regime} \\ 1 < W_d \; ; W_R < 1 & \text{Chain orientation regime} \\ W_R > 1 & \text{Chain stretch regime} \end{array} \qquad (10)$$

Most of the simulations we report are in the orientation and stretch regimes with very few occurring in the linear regime, which is asymptotically simply the Stokes solution, since the Rolie-Poly equation reduces to the Newtonian viscous fluid in this limit. [32]

The long-term aim of the research programme in which this work is situated, is to be able to predict and understand extrudate swell of complex, industrially relevant polymer melts. In order to understand these systems we start by predicting extrudate swell for a simple monodisperse, linear polymer melt, comparing with experiment, and building up in

complexity gradually. In this work we present fluid dynamics simulations using the Rolie-Poly constitutive equation, computed in 2D axisymmetric constriction and extrusion flow using the Lagrangian viscoelastic solver *flowSolve*. In section II.A we review the molecular model adopted for monodisperse polymers in non-linear flow, in section II.B the flow-solving protocol and in section III our experimental technique and materials. The results of comparing experiment and theory is presented in section IV, and conclusions in section V.

II. COMPUTATIONAL

A. THEORY

The theory used for the flow simulations is the finite-stretch Rolie-Poly constitutive equation. A modified version of Equation (7) was used to include finite extensibility for the single stretching Rolie-Poly element used in our models of the monodisperse melt and the two stretching elements used in our models of the bidisperse melt:

$$\frac{d\mathbf{A}}{dt} = \boldsymbol{\kappa}\cdot\mathbf{A} + \mathbf{A}\cdot\boldsymbol{\kappa}^T - \frac{1}{\tau_d}\left(\mathbf{A} - \lambda^2\mathbf{I}\right) - \frac{2}{\tau_R}\left(\frac{F(\lambda)-1}{\lambda}\right)\mathbf{A} - \frac{2\beta}{\tau_R}\left(\frac{F(\lambda)-1}{\lambda}\right)\frac{F(\lambda)}{\lambda^2}\left(\mathbf{A} - \frac{\lambda}{F(\lambda)}\mathbf{I}\right)$$

where

$$F(\lambda) = \lambda\left(\frac{\lambda_{\max}^2 - \lambda^2/3}{\lambda_{\max}^2 - \lambda^2}\right)\left(\frac{\lambda_{\max}^2 - 1}{\lambda_{\max}^2 - 1/3}\right) \tag{11}$$

and

$$\boldsymbol{\sigma} = {}^{F(\lambda)}\!/_{\lambda}\,\mathbf{A}$$

A is the chain orientation tensor and *F(λ)* is a 'spring force', reducing λ at times when the chain is significantly stretched.[33] Equation (8) was used to give non-linear constitutive structure to the remaining linear relaxation modes, which are all taken to be non-stretching in our flow regimes.

The value of λ_{max} used is 5, taken as a reasonable estimate for polystyrene as in [34]. This takes account that at very high shear a polymer chain cannot be stretched infinitely. Incorporating finite extensibility is vital in these simulations, in which the Rouse Weissenberg number is exceeded.

B. SIMULATION

The extrusion simulations are all calculated using the *flowSolve* software described above using the initial geometry and starting mesh of triangles shown in Fig. 1.

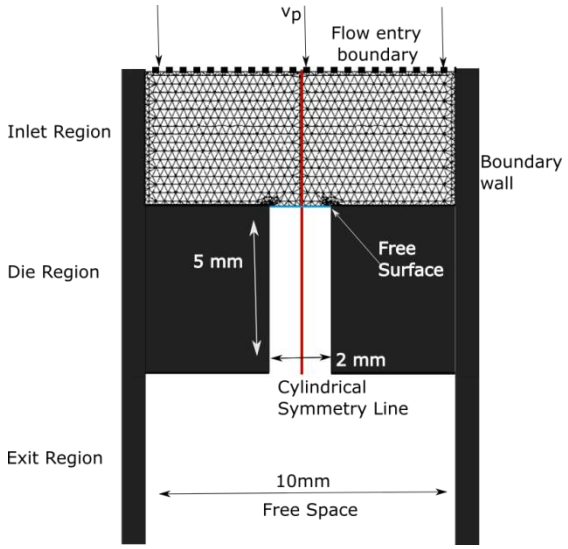

FIG. 1 The starting geometry and mesh used in a flowSolve extrusion simulation.

The geometry is defined to match the capillary available within the MPR, i.e. an upper well of diameter 10 mm, a capillary of length 5 mm and diameter 2 mm followed by free space. The simulations are all carried out within a cylindrical geometry using a central symmetry line. The full height of the upper test section and piston barrel within the MPR cannot be simulated due to the size of the geometry required therefore the upstream geometry is approximated using a flow entry line across which new triangles enter the simulation area at a defined velocity, v_p. The simulations all include gravity acting downwards with the polymer flow and a surface tension of 30 mNm^{-1} (taken from [35] at 180 °C.) acting on the free surface, even though these are calculated to be small effects for all but the lowest input velocities.

The number of points used in a simulation is characterised by the maximum length of a triangle size. This parameter was fixed at 0.3 mm in this study, after a series of simulations checking convergence, as this is a reasonable trade-off between accuracy and run-time. The effect of reducing the mesh size is minimal, a difference of ~1% versus a maximum length about half the size. Increasing the mesh size only has a significant effect at low shear rates, resulting in greatly increased swellings. At higher shear rates the swelling ratios obtained are

almost identical regardless of mesh size. This is detailed in Fig S1 of the supplementary information.

The parameter used to characterise the swelling in this work, as in most previous studies, is the *B* value, i.e. the diameter of the extrudate relative to the diameter of the capillary. The *B* value is calculated using the maximum width of the 'steady state' profile as a function of distance from the die exit. This is also the point where the initial rapid expansion versus time of the extrudate out of the die has stopped. An example plot of the evolution of the extrudate diameter with time, together with examples of extrudate profiles, is shown in Fig. 2.

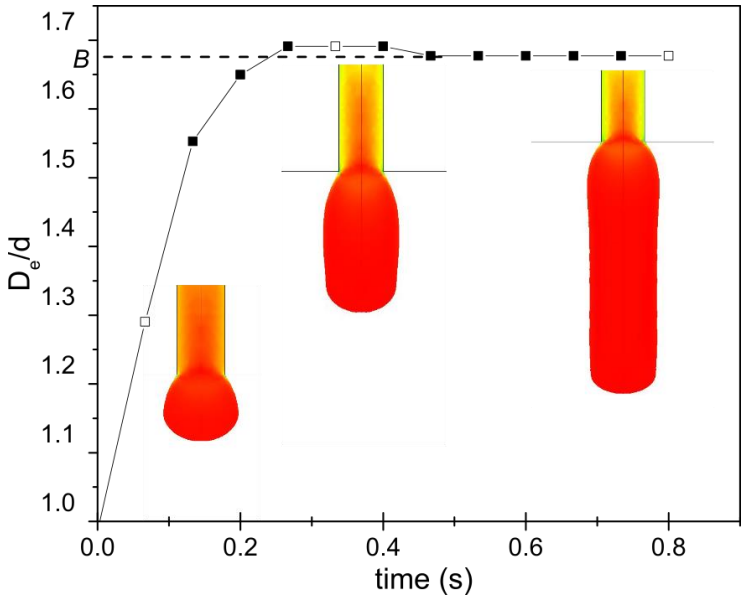

FIG. 2 A plot of simulated extrudate diameter versus time for PS281 at W_R=14. The maximum distance of the extrudate away from the centre line of the die is taken as D_e and the *B* value is the value of D_e/d where the graph becomes steady. The insets show the full extrudate profile at each open symbol.

In some cases, the polymer may initially expand outwards further than its steady state value. The extrudate is then pulled downwards and the swelling ratio decreases to a plateau. In this case the value at the plateau is still taken to be the swelling ratio. This overshoot is a small effect and is not systematic as a function of flow speed or Weissenberg number.

The parameter changed in the simulations is the flow input velocity v_p. This is the average velocity at which mesh points enter the simulation area across the radius of the flow entry boundary r_p. This is related to the equivalent Newtonian wall shear rate $\dot{\gamma}_w$ via the flow entry volume flux, *Q*:

$$\dot{\gamma}_w = \frac{4Q}{\pi r_{capillary}^3} \quad \text{where } Q = \pi r_p^2 v_p \tag{12}$$

Note that, due to shear-thinning, the true shear rate at the wall will be greater than (though of the same order as) this equivalent Newtonian shear rate. A range of shear rates were used corresponding to Weissenberg numbers relative to both Rouse and reptation times above and below 1. The range of input speeds required to span the same range of Weissenberg numbers changes depending upon the molecular weight although the speeds used for the 281 kDa polystyrene are 0.025 mm s^{-1}-10 mm s^{-1}.

III. EXPERIMENTAL

A. MATERIALS

The polystyrenes used were synthesised via anionic polymerisation. The samples PS100/PS400 were synthesised on a 200 g scale according to the procedure previously reported in [27]. The sample PS281 is partially deuterated and prepared according to the procedure reported in [15]. P627-S was obtained from PolymerSource and was prepared by living anionic polymerisation in THF at -78 °C.

A summary of the materials used in this paper is shown in Table I:

TABLE I A description of the polystyrenes used in this study and the molecular parameters used to define them at 180 °C, and to build optimised monodisperse models. τ_d is the terminal reptation time and Z is the number of entanglements per chain. *P627-S is bidisperse so its M_w is listed both as an average and (in parenthesis) for the higher M_W peak alone. The values of Z, τ_d and τ_R fitted to the linear rheology to create an optimatl monodisperse model for this polymer (results in figure 17) correspond to the higher M_W component alone. Parameters for a bidispese model for P627-S are given in Table II.

Sample Code	Molecular Weight (M_w) /kDa	M_w/M_n	Z	τ_d /s	τ_R /s
PS100	99.7	1.04	6	0.087055	0.017852
PS281	281	1.13	17	0.7648	0.04703
PS400	460	1.05	28	10.985	0.29276
P627-S*	252 (340)	1.27	21	4.4346	0.16285

A GPC characterisation was then performed on the three polymers used within the MPR. The samples were all run using THF as the solvent at 35 °C. The Viscotek TDA 302 instrument used a triple detector system with intensity, viscosity and RALS light scattering detectors to determine the molecular weight distribution.

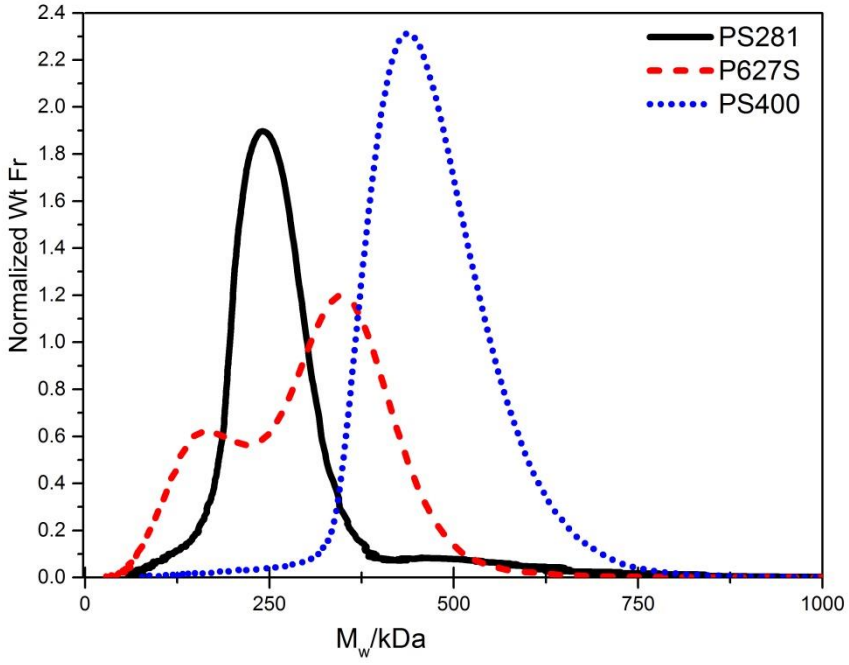

FIG. 3 GPC Data for the three polymers used in the MPR. This illustrates the bimodality of P627-S.

Fig. 3 shows that P627-S is bimodal with two peaks in the GPC. The data for the two peaks and parameters used to describe them are described in Table. II. The relaxation times used in simulations for these fractions are also included in this table and the method used to obtain these is discussed in Section III.B.

TABLE II Modelling data for the two Rolie-Poly stretching elements for the bidisperse model used in simulations of polymer P627-S at 180 °C.

Rolie-Poly Element	Molecular Weight (M_w) /kDa	Dispersity	Weight fraction, ϕ	Z	τ_d/s	τ_R/s
1	160	1.034	0.37	10	0.9256	0.03614
2	340	1.148	0.63	21	4.4346	0.2585

B. TECHNIQUES

Shear Rheometry experiments were performed using a TA instruments HR-2 rotational rheometer. A 25 mm plate-plate geometry with a sample thickness of 1 mm was used in all experiments. A frequency sweep was performed on each material using a frequency range of 0.1 - 600 rad s^{-1} and a temperature range of 140 °C - 200 °C. The data were time-temperature shifted using the *RepTate* software.[26]

The TTS parameters used are shown in Table III:

TABLE III WLF shift parameters at 180 °C for the polystyrenes used in this study.

Sample Code	Molecular Weight (M_w) /kDa	*C1*	*C2*	*C3*
PS100	99.7	7.63	-11	10.0
PS281	281	6.43	-11	16.0
PS400	460	7.64	-11	10.0
P627-S	252	7.63	-11	10.0

The data were TTS shifted to 180 °C to obtain the linear response of the polymer over a wide enough frequency range and then modelled using the linear theory of Likhtman and McLeish (Equation (6)) to obtain the τ_d and τ_R values given in Table I, from the terminal times of the rheology. *Z* values for the degree of entanglement of each sample were calculated using a uniform value for the entanglement molecular weight (M_e) of 16.5 kDa for the polystyrenes in this study.

The complete linear rheological spectra were modelled using a spectrum of 10 Maxwell modes, shown in Fig. 4 where the lowest frequency (slowest) Maxwell mode is assigned the relaxation time given in Table I.

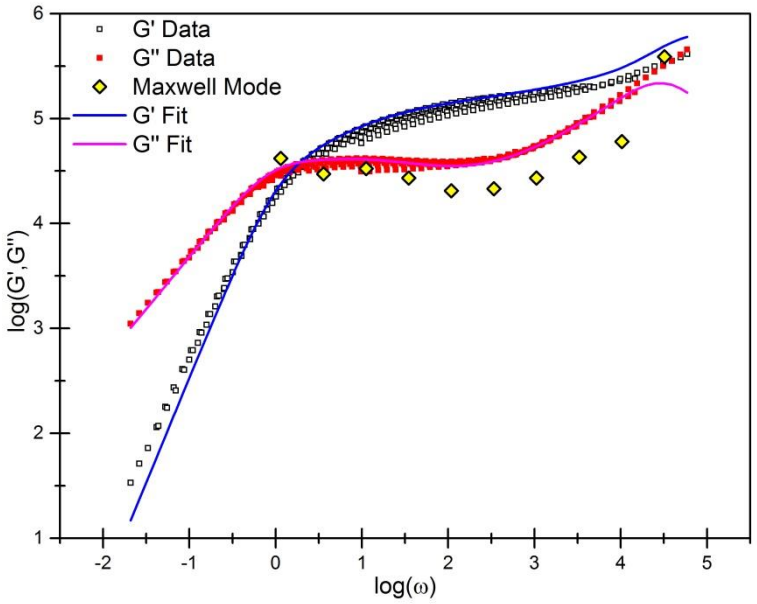

FIG. 4 An example spectrum of Maxwell modes (diamond symbols give their moduli and frequencies) fitted to linear rheometrical data for PS281 at 180 °C. The range is chosen to match the range of shear rates used within the simulations.

The non-linear rheology is approximated by assigning the single Rouse time from molecular theory to the slowest Maxwell mode, so creating a Rolie-Poly element in the constitutive model. This is an effective approximation to the full theory for a monodisperse, linear polymer as for these systems the slowest Rouse mode is the only one with a significant effect on the non-linear rheology. Further stretching modes would be required for a fit of polydisperse or branched systems as discussed in Section IV.D

The bidisperse polymer P627S was also modelled by a similar procedure, by using the first and second crossover-frequencies in the linear Maxwell-model fit to the linear rheology to obtain an estimate for τ_e and thus using Equation (6) to calculate τ_d and τ_R. The fitted reptation (terminal) time of the blend corresponds to the contribution of the higher molecular weight component alone, and the value of τ_R shown in Table I is the 'bare' Rouse time that this fraction would possess in a monodisperse melt. For a more accurate description of the non-linear rheology the entanglement-physics effect of bimodality was considered. Read et al [36, 37] showed that in a bimodal blend, constraint release within the 'fat' tube (constraints formed from entanglements with the high molecular weight chains alone) greatly increases the effective stretch-relaxation time (Rouse time) of that fraction in accordance with the formula:

$$\tau_{R,new} = \frac{\tau_R}{\phi_{long}} \tag{13}$$

where ϕ_{long} is the volume fraction of long chains in the blend. The Rouse time of the 340 kDa chains, when a component in the bidisperse blend, will therefore be increased significantly from its monodisperse value, and thus its chain stretch will both relax significantly slower, and occur at lower extension rates than expected from the Rouse time given in Table I. This means that although the Rouse time of the short chain polymer is not exceeded the effective Rouse time of the long polymer is greatly exceeded at most experimental rates, and significant chain stretching occurs, causing extrudate swell.

A Rolie-Poly stretching element (Equation 7) with an inflated Rouse time, corresponding to the high M_W component, was therefore used to model the higher fraction in the bidisperse melt in the *flowSolve* simulations. The longest Rouse time of this high M_w component (of bare value 0.16285 s in Table I) was increased to take into account stretch time enhancement of the longer chain in accordance with Equation (13) where ϕ_{long} is the weight fraction of the 340 kDa chains in the blend. This gives the renormalised Rouse time used in simulations of 0.2585 s shown in Table II. A second stretching mode was added with Rouse time corresponding to the predicted values for the smaller molecular weight corresponding to the pure component peaks. These two Rouse times were calculated from Equation (6) (and adjusted according to Equation (13) in the case of the slower mode) and Z values calculated from the GPC peak molecular weights and the M_e for the sample of 16.5 kDa. The reptation times and moduli were taken from the Maxwell mode fit for P627S, The weight fractions in Table II were calculated by integrating under each peak and using the ratio of the area under each peak to the total area as the weight fraction.

Extrusion experiments are performed using a Multi-Pass Rheometer (MPR). The advantage of this method is that only small quantities (~5-10 g) of polymer are required, allowing well characterised, monodisperse samples to be used rather than larger quantities of less well-characterised or more polydisperse samples. In these experiments, the MPR is used in a 'single pass' mode effectively as a small volume capillary rheometer. The bottom piston is left fully lowered and the top piston is gradually lowered so as to extrude polymer through the test section into the bottom chamber. The advantage of this arrangement is that the extrusion can be carried out isothermally rather than extrusion into room temperature conditions in which case the extrudate will cool, reducing the observed swelling. A schematic

diagram of the test section used is shown in Fig. 5. Two semi-circular test pieces are pushed together to form a cylindrical die through which extrusion can occur.

The top chamber and the top piston barrel are filled with polymer and extrusion occurs into the bottom chamber. All of these parts are maintained at a constant temperature by an oil heating jacket. Observation of the extrudate profile is possible using the quartz viewing windows.

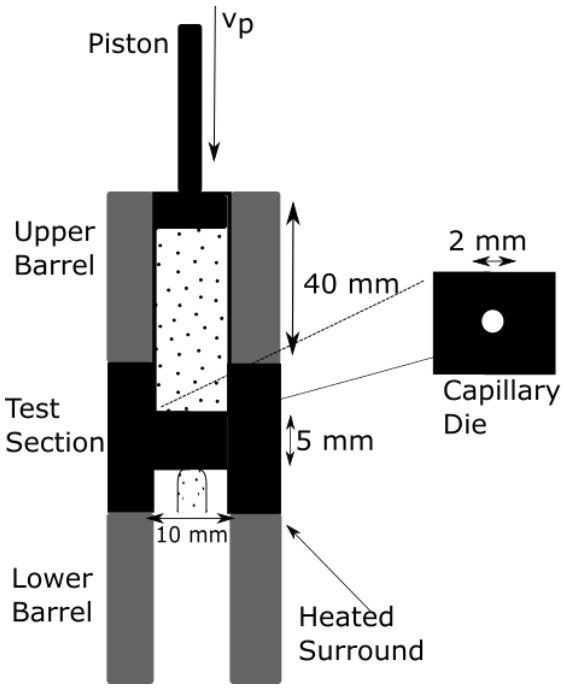

FIG. 5 The MPR capillary setup.

At the start of a test the polymer is packed into the upper test section and compressed to remove any inhomogeneity. The polymer is allowed to melt fully for a period of at least 30 minutes before extrusion. The temperature of the apparatus is maintained at 180 °C throughout the process. During a test the top piston is moved down and the polymer is pushed through the capillary into the bottom chamber where it can drop freely.

The diameter used for calculation of the *B* value is defined as the maximum extrudate width at steady state flow. (See Section II.B)

The small upper barrel size of 40 mm means that extrusion can only occur for a limited period of time. The maximum piston speed used varies per sample but allows for an extrusion time which is much greater than τ_d for all the polystyrenes studied meaning that the flow in the top barrel will have reached steady state during the extrusion. Gravity should also have a negligible effect upon the extrusion. Assuming the entire 5 g load of the upper well

were extruded into the bottom chamber and were hanging from the 2 mm diameter capillary under gravity the stress exerted would be in the order of 1.5×10^4 Pa. This is significantly less than the plateau modulus of the polystyrene of $\sim10^5$ Pa, so that the component of material strain due to gravity is small.

The extrudate form is very clear from the images. Transparency is limited in the materials of this study, as the low concentration of particulates that they acquire from the many passes necessary to the study creates strong absorption in the long dimension of the sample (out of the plane). To ensure that neither the accumulation of particulates, nor thermal degradation affected the melt rheological properties, the linear rheology was tested before and after extrusion, with no significant difference observed between the two tests.

Examples of the swelling observed in the MPR are shown in Fig. 6.

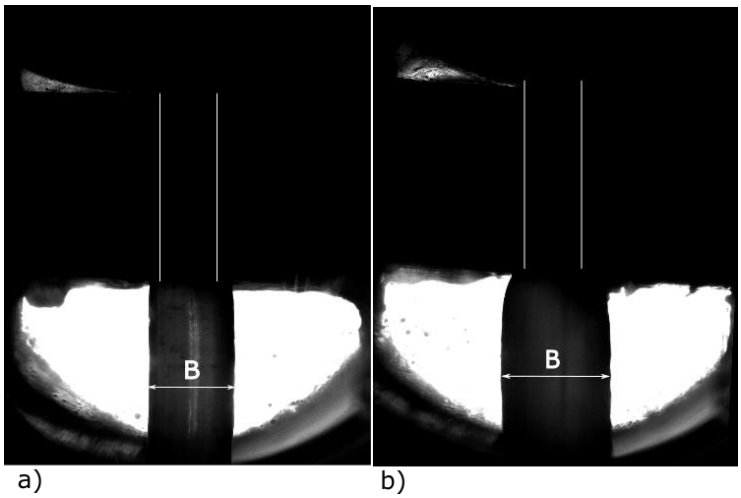

FIG. 6 Extrudate swell in the MPR at **a)** W_R=3.9 and **b)** W_R=46 respectively. The molten polymer is opaque therefore no detail can be seen in the upper chamber. The vertical white lines have been added to indicate the capillary diameter and the horizontal arrows indicate the maximum diameter (B value) for each.The extrudate continues to drop freely out of the viewable area into the lower chamber.

B values can readily be extracted from these images by measurement of the width of the extrudate at its steady state widest point using an image analysis program. It is also evident from the profiles in Fig. 6 that the extrudate swell grows considerably as the strain rates take the melt into the chain-stretching regime.

IV. RESULTS AND DISCUSSION

A. ROUSE AND REPTATION WEISSENBERG NUMBERS

Since a monodisperse melt possesses two relaxation times even at the coarsest level of approximation, there are two possible dimensionless deformation rates, depending on which timescale is used as a multiplier for the shear rate to make it dimensionless. We refer to these as the reptation and Rouse Weissenberg numbers defined in Section II.A. Once rates have been made dimensionless in this way, the only parameter that differentiates one monodisperse entangled melt from another is the ratio of Rouse to reptation times. This ratio is a single-valued function of the number of entanglements per chain, Z tabulated in Table I, so that $\tau_R/\tau_d \sim Z^{-1}$ for moderate degrees of entanglement. Plotting a property of melt flow such as the extrudate swell B against the reptation Weissenberg number for different molecular weights will superimpose features due to chain orientation, while plotting against the Rouse Weissenberg number will do the same for features arising from chain stretch.

The results for extrudate swell for the monodisperse polystyrenes used are shown versus equivalent Newtonian wall shear rate in Fig 7 (a), versus reptation Weissenberg number in Fig 7 (b) and versus Rouse Weissenberg number in Fig 7 (c).

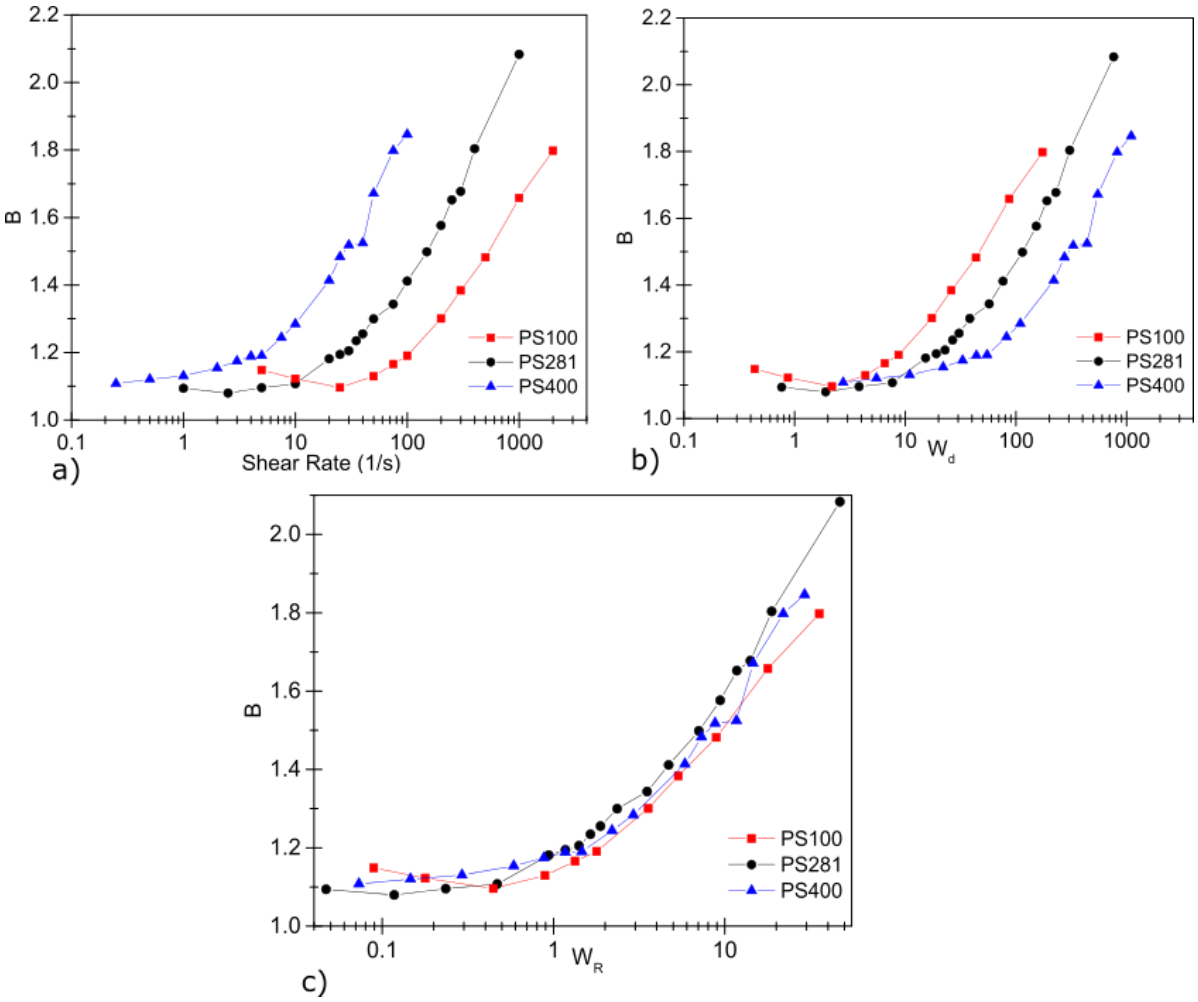

FIG. 7 Computed *B* values in flowSolve for three different molecular weight polystyrenes. **a)** Shows the data plotted as a function of equivalent Newtonian wall shear rate, **b)** shows the lack of superposition versus reptation Weissenberg number. and **c)** shows the superposition versus Rouse Weissenberg number.

At low Weissenberg numbers where there is almost no chain stretch there is a small decrease in *B* with shear rate. This is the first, very weak, non-linearity in the response of extrudate-swell. The data are consistent with the expectation that this sets in at reptation Weissenberg numbers of order unity. This minimum in swelling ratio is not constant with Rouse Weissenberg number but occurs at a roughly constant reptation Weissenberg number, meaning that this is a chain orientation rather than chain stretch induced phenomenon. No downturn is observed for PS400 as the reptation Weissenberg number is always exceeded within these simulations. Below W_d=1 the flow at the die exit has time to relax all the elastic stress built up at the die wall, leading to the limiting Newtonian result for the expansion. Above W_d=1, the reduction in apparent viscosity (both shear- and extension- thinning) that comes from chain alignment, results in an increased flow speed away from the die, compared with the low-flow case, reducing the swelling. This effect is consistent with early work by

Tanner on planar flows in which extrudate swell is seen to decrease below a Weissenberg number of 1. [38]

The swelling ratio at high shear rates is independent of molecular weight when plotted against W_R but there is no superposition versus W_d except at the lowest speeds where B is small and only weakly dependent upon W_R.

The superposition of the curves at different molecular weights versus W_R is very significant. This indicates that of the spectrum of relaxation times in the model the only one that makes a significant difference to the swelling is the Rouse time of the highest molecular weight fraction. Extrudate swell must therefore be a chain stretch phenomenon. An analysis at the underlying causes of extrudate swell may now be performed by looking at the chain stretch during the simulation.

B. CHAIN STRETCHING

The advantage of using fluid dynamics simulations combined with a molecular constitutive equation such as Rolie-Poly is that it is possible to look at the evolution of molecular variables such as chain stretch, as well as macroscopic ones, as a function of both time and location in the simulation. Fig. 8 shows the chain stretch as given by the value of λ within triangles adjacent to the capillary wall. The finite number of triangles present at the die wall results in some noise in the chain stretching data. The data in Fig. 8 and Fig. 10 are averaged over 5 triangles of the simulation mesh to produce smoother curves.

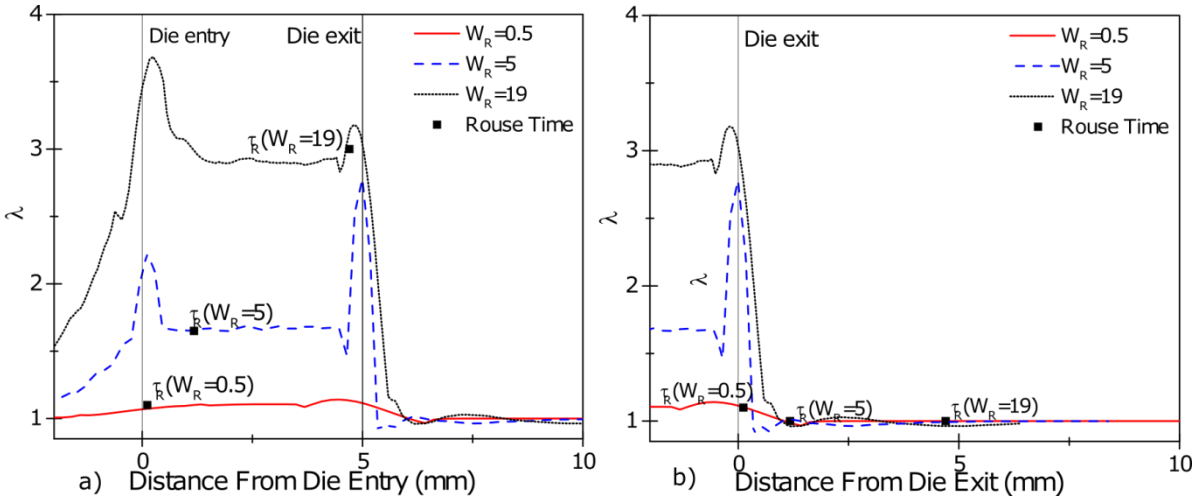

FIG. 8 Computed chain stretch along the die wall for PS281 at W_R above and below 1, keeping the die length fixed at 5 mm and the *l:d* fixed at 2.5. The distance the flow has travelled after τ_R, calculated from the mean flow velocity and the Rouse time is shown on each curve. The corresponding values for reptation are off scale

above $W_R \approx 3$ **a)** shows the flow in the before and after the die and **b)** shows an expanded view of the stretch relaxation after the die exit.

The chain stretch undergoes an initial increase towards the die entry, reaching a maximum at this point. This is due to the acceleration of the polymer flow from the well into the contraction. The chain stretch relaxes rapidly after the die entry and is followed by a period of constant stretch due to shear at the capillary wall, producing the plateaux features in Fig 8(a). Thirdly there is a sharp peak at the die exit. This is due to a strong extensional pull-off caused by the singularity at the die exit corner. This singularity is caused by the removal of the no-slip boundary wall condition and is always present even if the exit corner is rounded. The melt flow must leave the die wall at some point, which becomes a stagnation point for a local extensional flow. Lastly there is a period of rapid stretch relaxation upon which the stretch returns to approximately unity. At the higher shear rates the stretch drops below 1 briefly after the die exit. This is a reversing flow effect in which polymer chains are contracted slightly by the decelerating flow. Analysis of the chain stretch contour plot in Fig. 9 for a high flow speed highlights these features. The contours are most highly concentrated at the die entry and at the exit corner.

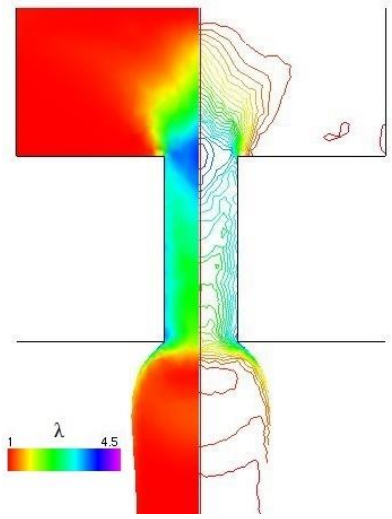

FIG. 9 Computed contour map showing chain stretch values for PS281 along the die for W_R=19. The contours are at an interval of λ=0.15.

This analysis reveals that the significant increase in stretch at the die exit, driven by the corner singularities, has a larger effect chain stretch than the accumulated shear flow at the capillary wall. Since this work also indicates that extrudate swell is primarily a chain stretch phenomenon, it is not correct to ignore the effects of the die exit as the stretch at the die exit will be much greater than that predicted from the shear rate at the capillary wall alone.

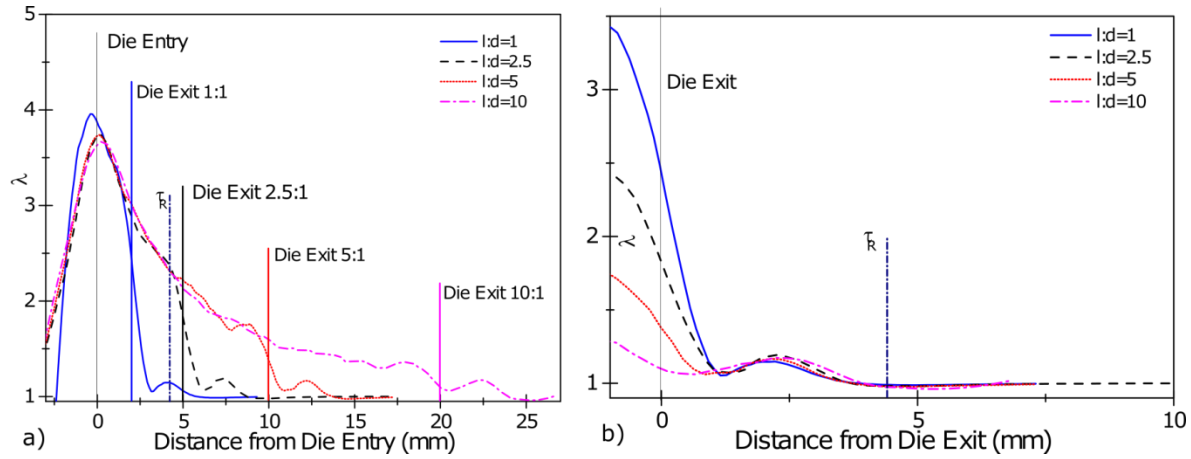

FIG. 10 Computed chain stretch at the centre line of the die for PS281 at W_R=19 for die lengths of 2, 5, 10 and 20 mm (*l:d* ratios of 1,2.5 and 10 respectively). The distance the flow has travelled after τ_R, calculated from the mean flow velocity and the Rouse time is shown as a vertical line. The corresponding value for reptation occurs at a distance of ~76 mm. **a)** shows relaxation of stretch before and after the die and **b)** shows an expanded view of stretch relaxation after the die exit.

Fig. 10 shows the chain stretch along the centre line for a variety of die lengths at W_R=19. The decay in chain stretch occurs on a timescale governed by τ_R therefore this timescale is shown on the graph rather than τ_d. Along the centre line there is an increase in chain stretch at the die entry followed by a period of stress relaxation along the die. The amount of unrelaxed stress at the die exit decreases, unsurprisingly, with increasing die length. This will increase the swelling ratio for short dies, although only for high shear rates. For the 5 mm die used in the MPR the flow cannot be said to have fully reached steady state within the die as some effect of chain stretching at the die entry remains at the exit. At lower speeds however, (below $W_R \cong 10$ for PS281) the die entry stretch will have decayed away before the die exit and the flow will have reached a steady state within the die. Any upstream flow effect is important at the centre line with no effect at the die wall. The chain stretch at the die wall has therefore reached a steady state value well before the die exit for all flow speeds. The die exit then has the effect of increasing the stretch at the die wall above the steady state value. Following the die exit there is a small peak in centre-line chain stretch where the material at the centre of the extrudate is stretched perpendicular to the flow direction by the expansion in this direction. This peak in stretch occurs at the point downstream of maximum swell and serves to pull the extrudate downwards slightly and lower the swelling ratio. As shown in Fig. 10 b) the position and magnitude of this peak do not depend upon the amount of unrelaxed stress at the die exit.

The evolution of the chain stretch in between the two trajectories of centre line and die wall interpolates between the two cases. Close to the die wall the stretch relaxes slightly along the

extruder before eventually reaching a steady state. Due to the increasing fluid velocity towards the centre line, the distance along the extruder required for chain stretch to relax to steady state increases with distance away from the die wall until the plateau features in chain stretch of Fig.8 to vanish completely and the profile for the 5:2 die shown in Fig. 10 is obtained. If the time the flow has spent within the die is calculated from the die length (of 5 mm) and the speed of the flow at a given radius, we can define a Rouse Deborah number for the flow at a specific radius:

$$D_R(r) = \frac{\tau_R}{\left(l \big/ V(r) \right)} \tag{14}$$

where the dimensionless radius r is the distance from the centre-line of the die divided by the die radius (of 1 mm), $D_R(r)$ is the Deborah number at radius r, l is the die length, and $V(r)$ is the flow velocity at radius r. At $W_R = 19$ $D_R(r)>1$ for $r<0.66$. This means that for the 5:2 die used within the MPR the flow within a distance of 0.34 mm of the die wall has had time to relax via Rouse motion within the die. This radius decreases with decreasing W_R until $W_R<10$ where even the flow at the centre-line has remained within the extruder longer than the Rouse time. The radius for reptation is closer to the wall than the diameter of a single simulation triangle and cannot be resolved.

C. EXTRUDATE PROFILE

The extrudate undergoes an initial expansion close to the die exit followed by a slight contraction after the maximum and then a period of roughly constant flow. The distance from the die at which the maximum B value occurs depends upon the flow speed. At speeds below the reptation Weissenberg number, the maximum occurs away from the die as the initial expansion due to chain stretching at the die exit is small. Between W_d and W_R there is a region where swelling is small and the maximum swelling ratio occurs almost immediately after the die exit. (Fig. 11(a)) At higher speeds, the initial expansion out of the die is large and so the maximum occurs further from the die exit. (Fig. 11(b)).

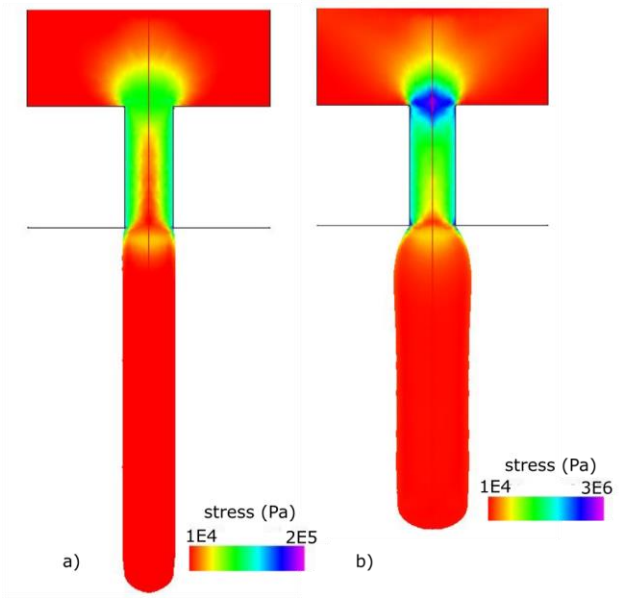

FIG. 11 (a) Simulated extrudate swell profile showing the magnitude of the stress tensor at W_R=0.23. **(b)** Simulated extrudate swell profile at W_R=14.

The predicted distance below the exit of the 5 mm long, 2 mm diameter die at which the steady state maximum occurs is shown in Fig. 12 as a function of W_R.

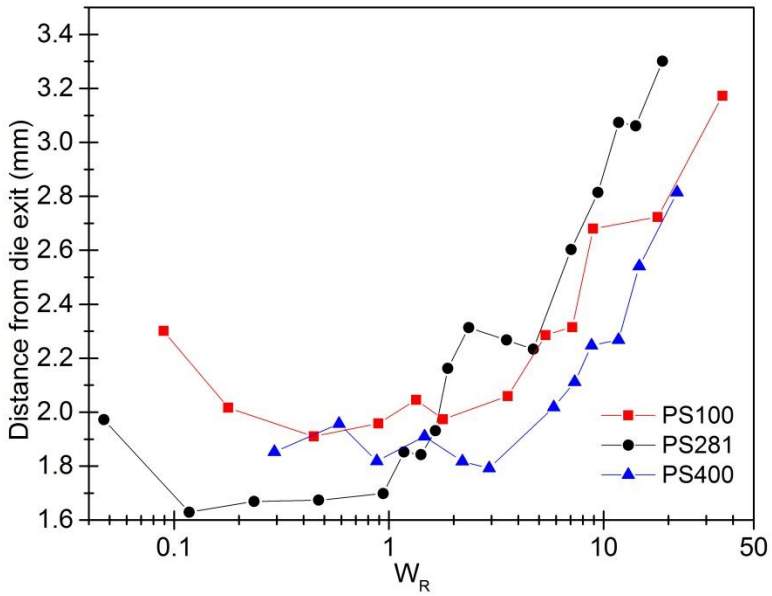

FIG. 12 The simulated distance below the die exit at which the maximum extrudate dimeter for the three polymers occurs. If the extrudate is flat for a long period then the lowest distance is plotted.

The observed distance below the die exit at which the maximum swelling occurs exhibits a minimum slightly above W_R and an increase after this point. The data for the three molecular weights show qualitatively the same trend although quantitatively differ significantly. This indicates that there is a flow driven element to this distance, i.e. how fast the flow can travel

the maximum outwards distance D_e as well as how fast the viscoelastic stress can relax after extrusion. Given that there is no intrinsic length scale to the viscoelastic properties of the fluid used as simulation inputs (barring gravity and surface tension effects) it would be expected that the distances in Fig. 12 would scale with die diameter, in the case that all velocities were scaled by the same factor. This process defines a similarity-scaling for extrudate-swell, connecting, by equivalence, experiments at different space and velocity scale (but equal time scale), and with equal B values and profiles.

It is impossible to take measurements at long distances away from the die exit within the current MPR setup. The viewable area is less than 5 mm therefore the maximum swelling ratio must be taken as the maximum reached within this window. This is not a large problem as the differences in diameter observed at distances far from the die in *flowSolve* are minimal and, as shown in Fig. 12, the maximum should always be reached by this point.

Our quantitative comparisons of simulation and experiment have used the single-parameter B as an effective summary measure of extrudate swell, but it is important to understand that the method allows for a prediction and comparison of the entire spatial profile of the extrudate. In particular, the results shown in Fig. 11 indicate that a qualitative change in the profile accompanies the different regimes of behaviour in the function $B(W_R)$. Example comparisons of the swelling profiles from theory and experiment in two different flow regimes are shown in Fig. 13.

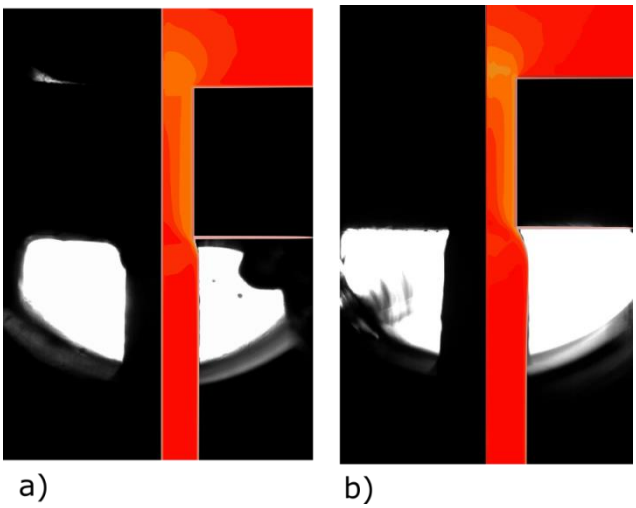

FIG. 13 Comparison of the swelling profiles obtained from simulation (right) and experiment (left) for PS281 at **a)** $W_R = 1$ and **b)** $W_R = 5$.

The simulated extrudate profile is roughly consistent with that from experiment. Some fluctuations in the extrudate diameter occur well below the die exit which are not predicted

by *flowSolve*. This is due to the onset of unsteady flow, known to occur at Rouse Weissenberg numbers greater than 1. [39] These fluctuations do not affect the magnitude of the swelling ratio however.

D. SWELLING RATIOS

Fig. 14 shows the results from the MPR compared with simulations.

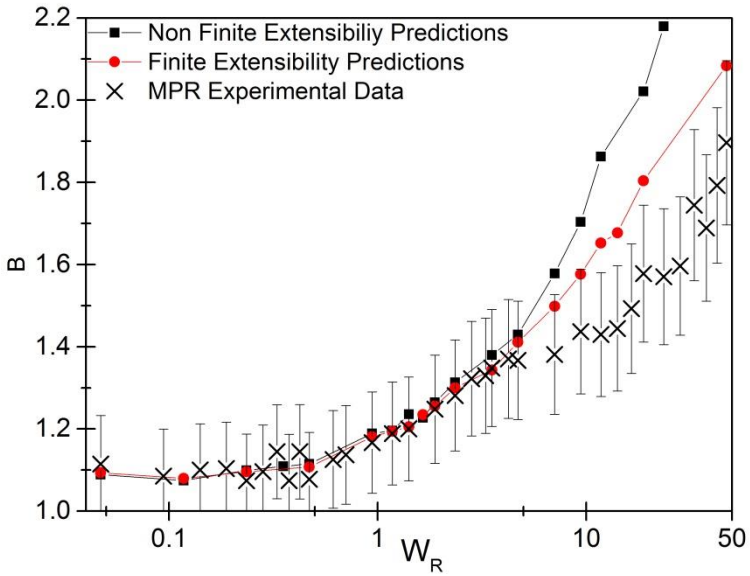

FIG. 14 Comparison of experimental data with theoretical predictions of extrudate swell for PS281 at Rouse Weissenberg numbers up to 50. Curves for finite and infinite extensibility predictions are overlaid on the data.

A good agreement is seen up to W_R~7 at which point the increase in extrudate swell with shear rate, $\frac{dB}{dW_R}$ slows down. The simulations do not predict this, instead predicting a continued increase in swelling. Above this point the shear rates are too high and the polymer begins to leak out around the sides of the geometry and around the quartz viewing windows. Despite this, the simulations still match the experiments accurately well into the chain stretching regime.

The effect of finite extensibility on the simulations is overlaid on Fig. 14. Without finite extensibility (using Equation (7) rather than Equation (11) for the stretching elements of the simulation) the simulations more quickly overestimate the swelling, failing to accurately model the swelling above W_R=5. The finite chain stretch both restricts the steady state stretch at the wall and greatly decreases the magnitude of the increase at the die entry and exit. The initial chain stretch peak height seen in Fig. 8 for W_R=19 is 3.3 whereas without finite extensibility it increases to 15. The exit chain stretch peak height increases from 3.1 to 9.9

upon the removal of finite extensibility. These increased chain stretch values obviously significantly increase the swelling ratios observed.

The results from both experiments and simulations can be compared to Equation (1). The Normal stress differences are calculated from the dynamic moduli of the polymer using the Laun approximation:[40]

$$N_1(\dot{\gamma}) \cong 2G'(\omega)\left[1+\left(\frac{G'(\omega)}{G''(\omega)}\right)^2\right]^{0.7} \tag{15}$$

where ω, the frequency of oscillation of the rheometer, equals $\dot{\gamma}$, the shear rate at the capillary wall.

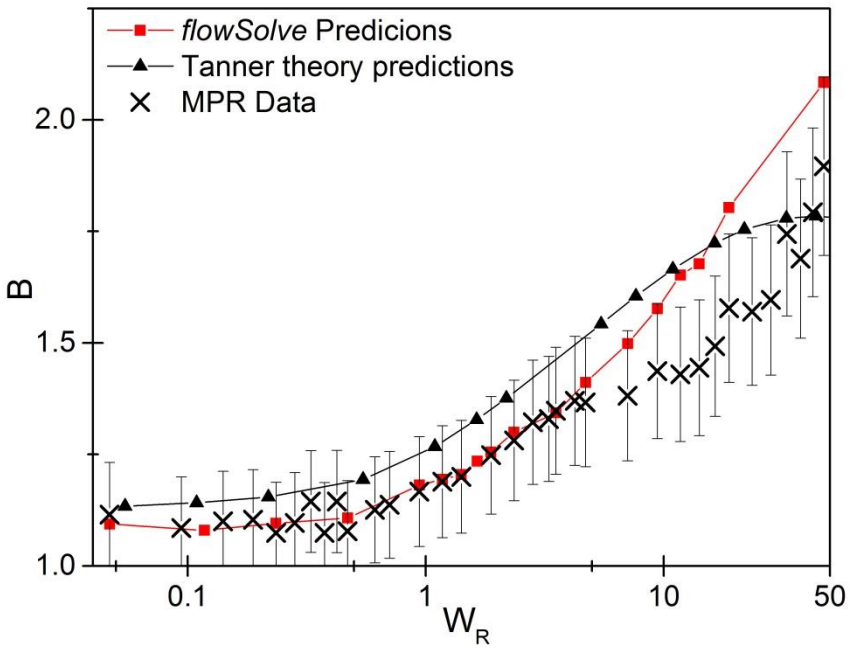

FIG. 15 Comparison of the theory of Tanner in Equation (1) to the monodisperse predictions of *flowSolve* and experimental data for PS281.

The Tanner theory qualitatively predicts the behaviour of the data, predicting an upturn in *B* at roughly the correct value. It does not predict the upturn at low shear and rapidly starts to over predict the extrudate swell above the Rouse Weissenberg number. *flowSolve* does a better job quantitatively predicting the extrudate swell for this system.

To check that this method worked for a different polymer the higher molecular weight polymer PS400 was used. A lower shear rate range was used so as to span the same range above and below the Rouse Weissenberg number. The results are shown in Fig. 16.

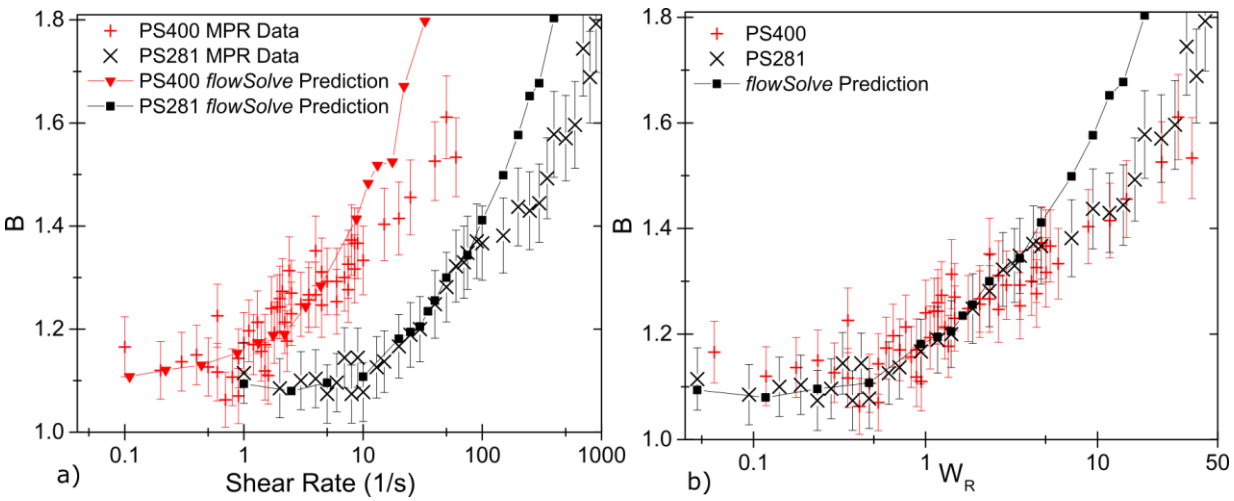

FIG. 16 Comparison of the extrudate swell data for PS281 and PS400. **(a)** shows the data versus the MPR equivaent Newtonian wall shear rate. **(b)** shows the data scaled using the Rouse Weissenberg number of the two polymers. Only one theory prediction is shown on this graph for simplicity.

The two data sets show the same trend, i.e. that the extrudate swell data falls onto a single curve when the shear rate is converted to the Rouse Weissenberg number. This confirms the *flowSolve* predictions from Fig. 7 where this single curve is predicted.

A third polymer, with bimodal dispersity, was used to compare with these results. The material used is the Polymer Source polystyrene P627-S which has a similar M_w to PS281 although a higher dispersity (See Table I) Analysis of the GPC data in Fig. 3 for the polymer shows that it is bimodal, with a peak at M_w=340 kDa and a smaller peak at 160 kDa. The extrudate swell results obtained for the bidisperse polymer are shown in Fig. 17 alongside the monodisperse prediction from *flowSolve* (using the parameters of Table I).

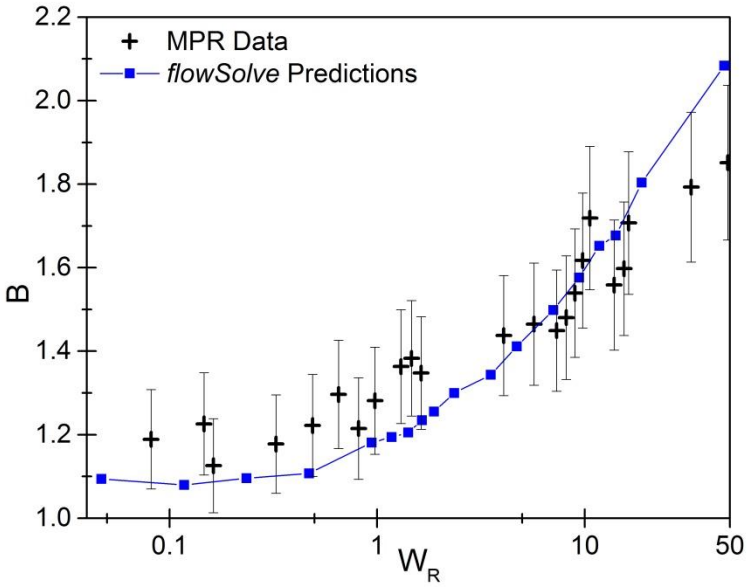

FIG. 17 Comparison of theoretical predictions for a monodisperse polymer of M_w 340 kDa corresponding most closely with the experimental data for the bidisperse polymer P627-S (parameters of Table I) The disagreement shows that the extrudate swell is very sensitive to molecular weight distribution.

The predictions for a strictly monodisperse polymer surprisingly agree better to the experimental data at higher Weissenberg numbers although, as expected, worse at lower Weissenberg numbers. This is attributed to the polydispersity of the polymer since any difference in molecular weight is insignificant when normalised to W_R.

It is therefore necessary to use an understanding of the different relaxation times in a bidisperse blend to predict extrudate swell. To this end, the adjusted relaxation times in Table II were used to give a bidisperse prediction.

A comparison of the data from the monodisperse and polydisperse polystyrenes is shown in Fig. 18. The two polymers have almost the same average number of entanglements so the difference is due to the polydispersity. The predictions for monodisperse and bidisperse polymers are overlaid on the data. It is evident from the improved agreement of the bidisperse prediction with the data at low W_R, that an inflated Rouse time as discussed in Section III.A is required for fitting this blend. Deviations are still seen at low W_R, which is likely to arise from the strict bimodal model we have used for this material, both of whose molecular weight distribution peaks are considerably broader than that of a model monodisperse sample. Although a molecular weight of 340 kDa is used for the long chain fraction a large number of chains are longer than this and would have a greater Rouse relaxation time.

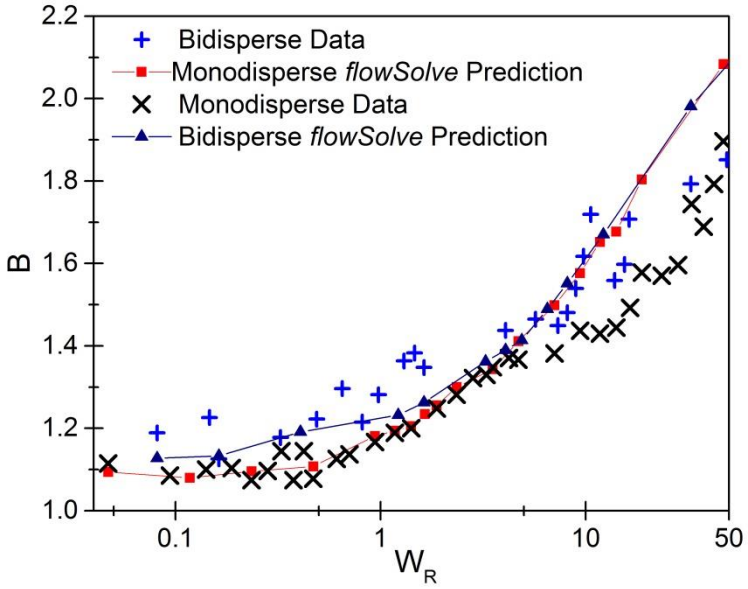

FIG. 18 Comparison of the experimental swelling from PS281 and P627-S polystyrenes alongside the *flowSolve* predictions for each. The Weissenberg numbers for each polymer are calculated separately using the Rouse times from Table I**.** In the case of P627-S parameters for the monodisperse model are in Table I and for the bidisperse model in Table II.

The greatest difference between the two experimental data sets is seen at W_R~0.6 with the data becoming closer at higher shear rates. The swelling ratios for the bidisperse case are consistently higher than that for the monodisperse case. This is due to the significant stretching of the long chains even at low W_R. The difference is smaller later as the 281 kDa chains begin to be stretched above their Weissenberg number.

V. CONCLUSIONS

We have shown that a fully nonlinear model derived from the tube theory of entangled polymer melts, when computed in an extrusion geometry, is able to give quantitative account of the extrudate swell in monodisperse and bidisperse melts. The use of monodisperse melts in both modelling and experiment allows features that are otherwise obscured by polydispersity to be resolved clearly. For example, a small reduction in extrudate swell from its Newtonian value occurs at flow rates that orient chains without any stretching. However, the most significant molecular feature generative of extrudate swell is chain stretch. The dominance of chain stretch generates data-collapse, to good approximation, as a function of the Rouse Weissenberg number of the flow. The swelling begins to increase as the Rouse Weissenberg number is exceeded, i.e. as chain stretch becomes significant, and swelling ratios fall onto a single curve beyond this point regardless of molecular weight. Accounting

for finite chain extensibility is essential in the prediction of extrudate swell above the Rouse Weissenberg number. Measurements of the swell profile in isothermal conditions within the MPR are well accounted for by the theory up to $W_R \sim 7$ although at higher flow speeds the theory over-predicted the swelling, even with finite chain stretch. This may be a signature of the dependence of monomer friction coefficient on chain orientation at high chain-stretching rates as discussed in [41].

The multi-scale and spatially-resolved approach additionally sheds light on both the molecular and spatial causes of extrudate swell. In particular, we find that a large contribution to the stress-state arises from the extensional flow at the die exit, rather than solely from accumulated shear stress within the die.

The single stretching-mode Rolie-Poly model used for parameterising the polymers in *flowSolve* simulations is only valid in the monodisperse case. Additional modes, either stretching or non-stretching are required for accurate representation of melts with broader molecular weight distribution. These modes may need to be fitted to extensional rheology to ensure accurate representation of the non-linearity of the polymer within *flowSolve*. In the case of a bidisperse melt, an additional longer effective stretching time was required to account for low-rate extrudate swell, consistent with tube model predictions of slowed-down stretch relaxation in such systems. Future work will involve incorporating the non-linear rheology of polydisperse systems and branching into the simulations and comparing this to associated extrusion experiments. This should provide another step up in complexity toward that required for simulation of industrial melts.

SUPPLEMENTARY MATERIAL

See Supplementary Material for the description of how simulation mesh size affects the swelling ratio measurements mentioned in Section II. B.

ACKNOWLEDGEMENTS

The authors would like to thank Dr Dave Hoyle and Dr Tim Nicholson for help with the *flowSolve* software, Carl Reynolds and Dr Stephen Boothroyd for experimental help and Professor Lian Hutchings and Jon Millican for providing and characterising the polymers. This work was supported by the Engineering and Physical Sciences Research Council CDT in Soft Matter and Functional Interfaces (SOFI), grant ref. EP/L015536/1.

References

[1] Tanner, R.I., "A theory of die-swell," J. Polym. Sci., Part B: Polym. Phys, **8**, 2067-2078 (1970).

[2] Tanner, R.I., "A theory of die-swell revisited," J. Non-Newton. Fluid, **129**, 85-87 (2005).

[3] Liang, J.-Z., "A relationship between extrudate swell ratio and entry stored elastic strain energy during die flow of tyre compounds," Polym. Test., **23**, 441-446 (2004).

[4] Liang, J.-Z., "Estimation of die-swell ratio for polymer melts from exit pressure drop data," Polym. Test., **20**, 29-31 (2000).

[5] Seriai, M., J. Guillet, and C. Carrot, "A simple model to predict extrudate swell of polystyrene and linear polyethylenes," Rheol. Acta, **32**, 532-538 (1993).

[6] Phuoc, H.B. and R.I. Tanner, "Thermally-induced extrudate swell," J. Fluid Mech., **98**, 253-271 (1980).

[7] Koopmans, R.J., "Extrudate swell of high density polyethylene. Part II: Time dependency and effects of cooling and sagging," Polym. Eng. Sci, **32**, 1750-1754 (1992).

[8] Yang, X., S.-Q. Wang, and C. Chai, "Extrudate swell behavior of polyethylenes: Capillary flow, wall slip, entry/exit effects and low-temperature anomalies," J. Rheol., **42**, 1075-1094 (1998).

[9] Konaganti, V.K., M. Ansari, E. Mitsoulis, and S.G. Hatzikiriakos, "The effect of damping function on extrudate swell," J. Non-Newton. Fluid, **236**, 73-82 (2016).

[10] Konaganti, V.K., M. Ansari, E. Mitsoulis, and S.G. Hatzikiriakos, "Extrudate swell of a high-density polyethylene melt: II. Modeling using integral and differential constitutive equations," J. Non-Newton. Fluid, **225**, 94-105 (2015).

[11] Tomé, M.F., L. Grossi, A. Castelo, J.A. Cuminato, S. McKee, and K. Walters, "Die-swell, splashing drop and a numerical technique for solving the Oldroyd B model for axisymmetric free surface flows," J. Non-Newton. Fluid, **141**, 148-166 (2007).

[12] Ganvir, V., B.P. Gautham, H. Pol, M.S. Bhamla, L. Sclesi, R. Thaokar, A. Lele, and M. Mackley, "Extrudate swell of linear and branched polyethylenes: ALE simulations and comparison with experiments," J. Non-Newton. Fluid, **166**, 12-24 (2011).

[13] Verbeeten, W.M.H., G.W.M. Peters, and F.P.T. Baaijens, "Differential constitutive equations for polymer melts: The extended Pom–Pom model," J. Rheol., **45**, 823-843 (2001).

[14] McLeish, T.C.B., "Tube theory of entangled polymer dynamics," Adv. Phys., **51**, 1379-1527 (2002).

[15] Graham, R.S., J. Bent, L.R. Hutchings, R.W. Richards, D.J. Groves, J. Embery, T.M. Nicholson, T.C.B. McLeish, A.E. Likhtman, O.G. Harlen, D.J. Read, T. Gough, R. Spares, P.D. Coates, and I. Grillo, "Measuring and Predicting the Dynamics of Linear Monodisperse Entangled Polymers in Rapid Flow through an Abrupt Contraction. A Small Angle Neutron Scattering Study," Macromolecules, **39**, 2700-2709 (2006).

[16] Bent, J., L.R. Hutchings, R.W. Richards, T. Gough, R. Spares, P.D. Coates, I. Grillo, O.G. Harlen, D.J. Read, R.S. Graham, A.E. Likhtman, D.J. Groves, T.M. Nicholson, and T.C.B. McLeish, "Neutron-Mapping Polymer Flow: Scattering, Flow Visualization, and Molecular Theory," Science, **301**, 1691-1695 (2003).

[17] http://www.ceb.cam.ac.uk/research/services/rheologycentre/cambridgempr. (accessed 13/03/17);

[18] Ferry, J.D., Viscoelastic properties of polymers,(John Wiley & Sons, New York, 1980),

[19] Likhtman, A.E. and T.C.B. McLeish, "Quantitative Theory for Linear Dynamics of Linear Entangled Polymers," Macromolecules, **35**, 6332-6343 (2002).

[20] Likhtman, A.E. and R.S. Graham, "Simple constitutive equation for linear polymer melts derived from molecular theory: Rolie–Poly equation," J. Non-Newton. Fluid, **114**, 1-12 (2003).

[21] Graham, R.S., A.E. Likhtman, T.C.B. McLeish, and S.T. Milner, "Microscopic theory of linear, entangled polymer chains under rapid deformation including chain stretch and convective constraint release," J. Rheol., **47**, 1171-1200 (2003).

[22] Marrucci, G., "Dynamics of entanglements: A nonlinear model consistent with the Cox-Merz rule," J. Non-Newton. Fluid, **62**, 279-289 (1996).

[23] http://www.bpf.co.uk/Sustainable_Manufacturing/Ancillary_Equipment/Microscale_Polymer_Processing.aspx. (accessed 30/09/16);

[24] http://www.irc.leeds.ac.uk/mupp/. (accessed 13/03/17);

[25] http://www.irc.leeds.ac.uk/mupp2/. (accessed 13/03/17);

[26] http://www.reptate.com. (accessed 13/03/17);

[27] Collis, M.W., A.K. Lele, M.R. Mackley, R.S. Graham, D.J. Groves, A.E. Likhtman, T.M. Nicholson, O.G. Harlen, T.C.B. McLeish, L.R. Hutchings, C.M. Fernyhough, and R.N. Young, "Constriction flows of monodisperse linear entangled polymers: Multiscale modeling and flow visualization," J. Rheol., **49**, 501-522 (2005).

[28] McLeish, T.C.B. and R.G. Larson, "Molecular constitutive equations for a class of branched polymers: The pom-pom polymer," J. Rheol., **42**, 81-110 (1998).

[29] Lee, K., M. Mackley, T. McLeish, T. Nicholson, and O. Harlen, "Experimental observation and numerical simulation of transient “stress fangs” within flowing molten polyethylene," J. Rheol., **45**, 1261-1277 (2001).

[30] Auhl, D., D.M. Hoyle, D. Hassell, T.D. Lord, O.G. Harlen, M.R. Mackley, and T.C.B. McLeish, "Cross-slot extensional rheometry and the steady-state extensional response of long chain branched polymer melts," J. Rheol., **55**, 875-900 (2011).

[31] Clarke, N., E. De Luca, G. Buxton, L.R. Hutchings, T. Gough, I. Grillo, R.S. Graham, K. Jagannathan, D.H. Klein, and T.C.B. McLeish, "Chain Deformation in Entangled Polymer Melts at Re-entrant Corners," Macromolecules, **43**, 1539-1542 (2010).

[32] Bishko, G.B., O.G. Harlen, T.C.B. McLeish, and T.M. Nicholson, "Numerical simulation of the transient flow of branched polymer melts through a planar contraction using the `pom–pom' model," J. Non-Newton. Fluid, **82**, 255-273 (1999).

[33] Kabanemi, K.K. and J.-F. Hétu, "Nonlinear dynamics and conformational changes of linear entangled polymers using the Rolie-Poly model with an “effective” maximum contour length," Rheol. Acta, **48**, 801-813 (2009).

[34] Rolón-Garrido, V.H., M.H. Wagner, C. Luap, and T. Schweizer, "Modeling non-Gaussian extensibility effects in elongation of nearly monodisperse polystyrene melts," J. Rheol., **50**, 327-340 (2006).

[35] Wu, S., "Surface and interfacial tensions of polymer melts. II. Poly(methyl methacrylate), poly(n-butyl methacrylate), and polystyrene," The Journal of Physical Chemistry, **74**, 632-638 (1970).

[36] Auhl, D., P. Chambon, T.C.B. McLeish, and D.J. Read, "Elongational Flow of Blends of Long and Short Polymers: Effective Stretch Relaxation Time," Phys. Rev. Lett., **103**, 136001 (2009).

[37] Read, D.J., K. Jagannathan, S.K. Sukumaran, and D. Auhl, "A full-chain constitutive model for bidisperse blends of linear polymers," J. Rheol., **56**, 823-873 (2012).

[38] Tanner, R.I., "The swelling of plane extrudates at low Weissenberg numbers," J. Non-Newton. Fluid, **7**, 265-267 (1980).

[39] Hassell, D.G., M.R. Mackley, M. Sahin, and H.J. Wilson, "Experimental and Computational Identification of a Polymer Melt Flow Instability," AIP Conf. Proc., **1027**, 147-149 (2008).

[40] Sharma, V. and G. McKinley, "An intriguing empirical rule for computing the first normal stress difference from steady shear viscosity data for concentrated polymer solutions and melts," Rheol. Acta, **51**, 487-495 (2012).

[41] Ianniruberto, G., "Extensional Flows of Solutions of Entangled Polymers Confirm Reduction of Friction Coefficient," Macromolecules, **48**, 6306-6312 (2015).